PROCEEDINGS, Thirty-Fifth Workshop on Geothermal Reservoir Engineering
Stanford University, Stanford, California, February 1-3, 2010
SGP-TR-188

IMPACT OF GEOLOGICAL CHARACTERIZATION UNCERTAINTIES ON SUBSURFACE FLOW USING STOCHASTIC DISCRETE FRACTURE NETWORK MODELS

Souheil M. Ezzedine

Lawrence Livermore National Laboratory
National Security Engineering Division, L-188
7000 East Avenue, Livermore, CA 94550
e-mail: ezzedine1@llnl.gov, phone: 925-422-0565

ABSTRACT

A major issue to overcome when characterizing a deep fractured reservoir is that of data limitation due to accessibility and affordability. Moreover, the ability to map discontinuities in the rock with available geological and geophysical tools tends to decrease particularly as the scale of the discontinuity goes down. Geological characterization data include, but not limited to, measurements of fracture density, orientation, extent, and aperture. All of which are taken at the field scale through a very sparse limited number of deep boreholes. These types of data are often reduced to probability distribution functions for predictive modeling and simulation in a stochastic discrete framework. Stochastic discrete fracture network models enable, through Monte Carlo realizations and simulations, for probabilistic assessment of flow and transport phenomena that are not adequately captured using continuum models. Despite the fundamental uncertainties inherited within the probabilistic reduction of the sparse data collected, very little work has been conducted on quantifying uncertainty on the reduced probabilistic distribution functions. Using nested Monte Carlo simulations, we investigated the impact of parameter uncertainties of the distribution functions of fracture network on the flow using topological measures such as fracture connectivity, physical characteristics measure such as effective hydraulic conductivity tensor.

INTRODUCTION & PROBLEM STATEMENT

The logical steps that must be taken to complete an EGS reservoir project are (Figure 1): (1) finding and characterizing a site by drilling and logging exploratory wells; (2) creating the reservoir by drilling an injection well, stimulating the fractures and drilling extraction well(s); and (3) operating the reservoir by completing and verifying the circulation loop and installing operating equipment (DOE, 2008).

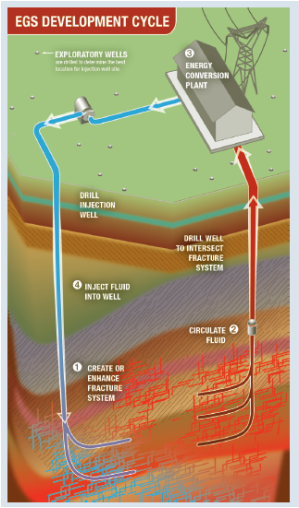

Figure 1: Logical steps to complete an EGS reservoir project (DOE, 2008)

Despite that geothermal energy is a mature geosciences energy technology, novel approaches have already been suggested, and some have been conceptually analyzed, (i.e., Tenma et al. 2003; Fujii 2004; Nalla et al. 2004; Porras et al. 2007). The use of alternative heat-transfer fluids in EGS has also recently gained considerable attention (i.e., Brown 2000; Pruess and Spycher, 2008; Pruess 2006; Gherardi et al. 2008; Kaieda et al., 2009). The success of old and new approaches remain limited by the sparse knowledge gained from the geological site characterization and the fundamental uncertainties inherited within the probabilistic reduction of the sparse data collected and their adequacy for the mechanical and chemical stimulation of geothermal systems (DOE, 2008). Furthermore, successful reservoir management and operation will rely heavily on how accurately models can predict reservoir behavior. Despite that design and predictive tools and codes (Pruess, 2008) exist very limited knowledge has been gained on their applicability and

validity of their assumptions. The objectives of the present paper are twofold: 1) assess the uncertainty associated with the geological site characterization and its impact on predictive results 2) and assess the uncertainties within model assumptions and dimension reduction. Both objectives are treated in a stochastic framework.

CONCEPTUAL MODELS OF POROUS FRACTURED MEDIA

Several different conceptual models have been used to describe flow and transport in fractured media. Several different approaches, or concepts, have been used to describe the fractured mass (Figure 2). Models can be roughly classified as equivalent porous media models (HPM), multiple interacting continua (SCM, MCM) such dual porosity models, and stochastic discrete fracture or pipe-flow models (DFN, PFN). One could also develop models that overlap these categories or transform one from the other such as the case of DFN and PFN.

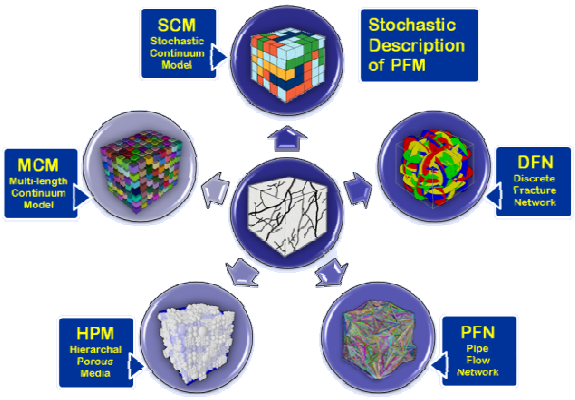

Figure 2: Stochastic description of Porous Fractured Media (PFM): equivalent hierarchal porous media (HPM) models, multiple interacting continua (SCM, MCM), and discrete fracture models (DFN, PFN).

None of the above conceptual pictures is "best" in an absolute sense. Rather, each may be appropriate for a particular situation or dictated by the limited available data. Models that are conceptually simpler have the advantage of being easier to implement as a rule, but they may also oversimplify the situation and miss important phenomena that are taking place. More complex models have the potential to provide a more detailed description of what is happening at the site being modeled, but they are also likely to be more difficult to implement and may require data that cannot be collected with currently geological and geophysical available techniques. Hereafter, we focus only on stochastic DFN models and their counter-part stochastic PFN models which are obtained through dimension reduction scheme described in the next section.

DESCRIPTION OF SELECTED APPROACHES

In DFN approach based on the model described in Ezzedine (2005), the fractures are treated as discs. The density and extensions are difficult to determine independently. There are relations between these magnitudes that can be used to test the connectivity of the medium (Charlaix et al, 1984). The hydraulic model is a bond model. The flow is two-dimensional in the fracture plane. Each mother-fracture can be mapped by daughter-fractures. Daughter-fractures are reduced to one dimensional bond (pipe). An additional parameter called *aperture* is assigned to each disc in the model (Figure 3).

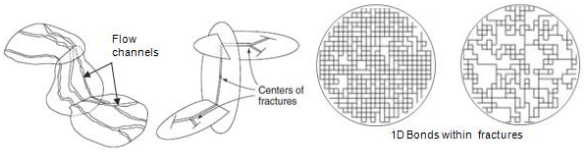

Figure 3: Example of dimension reduction of a fracture network (Modified from Ezzedine, 2005).

Geometry of Fracture Network

The geometrical model assumes that the fractures are finite and can be assimilated to simple elements such as discs (Figure 4a) or polygons whose geometric properties, distribution in space, direction and extension can be sampled on the basis of probability distributions deduced from structural observations on the site (Dershowitz et al., 1988). It is assumed that the stationarity hypothesis is satisfied and these magnitudes are not taken to be regionalized variables. In this approach, Ezzedine (2005) the fractures are treated as discs. In natural networks, fractures can usually be divided into families of defined by their average main direction. For a given realization, fractures are drawn sequentially for one family of directions at a time. The families are then combined to create the final fracture network (Figures 4b,c). For a given family, the stochastic generation can be made as follows:

- **Number of fractures**: A Poisson process is used to obtain the number of discs belonging to a specific family in the simulated volume as a function of the volumetric density of each family of fracture
- **Location of the disc centers**: The centers of the discs are distributed following a uniform distribution in the domain of interest.
- **Orientation**: The direction of a fracture is defined by its normal unit vector. The families of directions in a network consist of fractures with similar directions. Their normal vectors form an approximately cone-shaped segment, the axis of which is the pole of the family. Several probability

distribution functions are available (e.g. Fisher).

- Radius: The "radius" is the parameter describing the extent of the fracture and it is by far the most difficult one to determine. Several statistical laws are available to describe radius distribution (e.g., normal, log-normal, power-law).

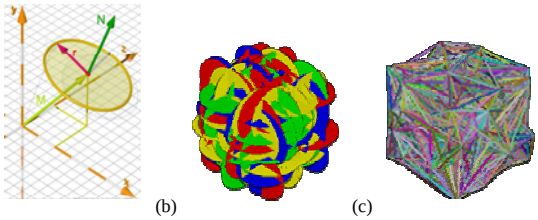

(a) (b) (c)

Figure 4: a) Each fracture is parameterized by its location (center, M), orientation (normal, N), size (radius, r) and thickness (aperture). Each family of fractures is defined by its density and orientation. Example of SDFN (b) and SPFN (c), one is correlated to the other. SPFN is obtained by erosion (reduction) of fractures to connected pipes.

Connectivity

The analysis of the connectivity and the search for continuous paths within such fracture networks use algorithms shared with graph theory and domain decomposition techniques. In fact, it is easy to ascertain whether two fractures are interconnected or not but, in a network of fractures it becomes very CPU time consuming to examine all the pair of fractures. Therefore, the flow domain is decomposed into sub-domains. A given disc intersects one or several of these elementary volumes. Two discs will not cut across each other unless both of them together cross at least one of the blocs. This method makes it possible to limit the number of tests. Details of the implementation are given elsewhere (Ezzedine, 1993).

Steady and Unsteady Flow Models

The flow is not two-dimensional in the fracture plane but occurs in channels linking the centers of the connected discs. The walls are impervious. The unsteady-state fluid model is based on the first and the second Kirchoff Laws. Applications of the both laws lead to a linear equation system of the heads at the center of the connected fractures. The transient flow model is based on the solution of the diffusion equation in one dimension in a bond by means of the Laplace transform (despite that it was first published by Barker, 1991, it was implemented by Ezzedine early 1989). The method is used on all the bonds, taking into account the continuity between the connected nodes and resulting in a linear equation system in the Laplace transform domain of the node heads. To solve this at each time step, one needs a numerical inverse Laplace transform of the node heads, which is obtained with Talbot's algorithm (1979).

THE APPROACH: NESTED MONTE CARLO SIMULATION

To summarize the problem in statistical terminology, the geometrical (geological) model is a stochastic one while the flow problem is solved deterministically within the stochastically generated fractures (S/D approach). It is however possible to adopt stochastic framework to solve the heat and mass transport in the fracture network using for example particle tracking or random walk scheme (S/S approach). The current model can handle both; however for the present study we limit ourselves to S/D approach. Statistically speaking, each SDFN characterized by:

- Density model (i.e. Poisson process) defined by its mean density and its variance (congruent models)
- Orientation model (i.e. Fisher) defined by truncated random distribution of the mean and variance
- Aperture model (i.e. Normal, Log-Normal) defined by truncated distribution of the mean and variance
- Radius model (e.g. Power-Law, Normal) where the parameters of the model are defined by truncated distribution with random mean and variance
- Number of family of fracture which in turns impact the statistical models of each of the previously listed parameters and the final composition of the fracture network itself.

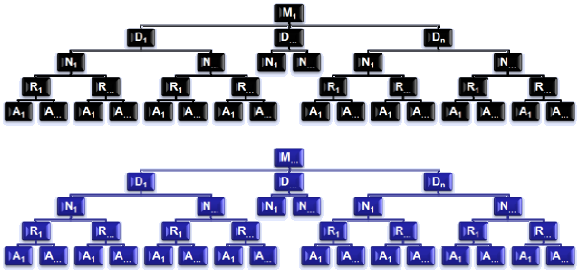

Figure 5: Example of a nested Monte Carlo simulation scheme where each fracture model (M_i: e.g. blak, blue) is characterized by its density (D_i^j), its normal (N_i^j), its radius (R_i^j) and its aperture (A_i^j). The center of each fracture is omitted in the figure but embedded in the density step level.

As one can expect, the space parameters is very large and therefore the number of simulation is exorbitant (Figure 5). Despite that LLNL possesses computer clusters with large number of nodes, a nested Monte Carlo sampling scheme is adopted and the space of parameters is refined as needed based on information-entropy criteria. This enables the current

simulation framework to be adopted on a small number of nodes rather than a brute-force solution. The details of the algorithm are beyond the scope of the present paper, however details can be found in Ezzedine, 2008 & 2010.

As it has been previously stated, the size (e.g. radius) of the fracture is by far the most difficult one to ascertain. The first moments of fracture radius are hard to obtain from spatially scattered, sparse exploratory boreholes. Moreover, the number of family of fracture is by no mean a deterministic problem. Therefore, high uncertainties are associated with their statistical distribution law, its mean, variance to name a few. Thus, in the present paper we focus our efforts on assessing the uncertainty associated with the fracture radius and we refer the readers to Ezzedine, 2010 for a more complete analysis of the parameter space.

SIMULATED CASES

The domain of interest is a cube of $(10^3)^3$ m^3 with all lateral surfaces specified as 1st type boundary condition set at a pressure of 10m while the injection well is centered in the simulation volume (Figure 6 Left). A second case is simulated with similar setup except that the top and bottom sides of the domain as impervious (Figure 6 Right). The injection interval length is 100m and it is set at a pressure of 1000m for both simulation cases.

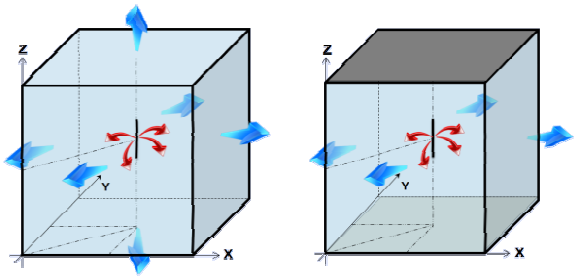

Figure 6: Simulated cases: Left) all sides are 1st type boundary conditions (blue arrows); injection well is centered in the domain (black segment) and it is set as a 1st type boundary condition. Right) only lateral sides are 1st type boundary conditions. Top and bottom sides are impervious.

The statistical description of the fracture network is given in Ezzedine (1994). The goal is to populate the simulation domain with a 100 SDFN based on the statistical average of the "ground-truth", i.e. the mean radius of the fractures is "known" and set to be equal to R_0 (Figure 7). Then each of SDFN mean radius $\langle R \rangle$ is increased or decreased by a factor of 5% such that $\langle R \rangle / R_0$ span from 0.5 to 1.5, that is a 50% decrease to 50% increase of R_0. Each 100 SDFN are then re-run 20 times. The 1st and 2nd statistical moments of the in-fluxes (red arrows in Figure 6) and out-fluxes (blue arrows in Figure 6) are calculated. The 1st moment for each $\langle R \rangle / R_0$ case is then renormalized to the 1st moment correspondent to the "ground-truth" mean flux, i.e. $\langle q \rangle / q_0$. Similarly the 2nd moment of each $\langle R \rangle / R_0$ case is also renormalized to "ground-truth" 2nd moment, i.e. σ^2_q / σ^2_0. Here q_0 and σ^2_0 are the mean and the variance of the "ground-truth" case, respectively.

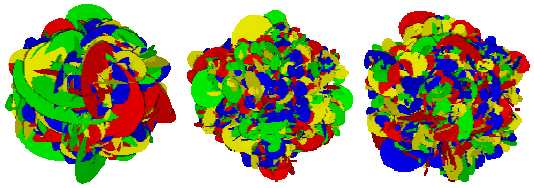

Figure 7: Example of SDFN used for flow simulation

RESULTS & DISCUSSION

Results of the 1st and 2nd moments are plotted as function of the scaling ratio $\langle R \rangle / R_0$ for both simulated cases.

Case I: Sides are 1st type boundary conditions

Not surprisingly, the normalized mean fluxes, from each side of the domain, are generally increasing with the alteration ratio, $\langle R \rangle / R_0$. The larger mean radius $\langle R \rangle$ compared to the ground-truth radius R_0, the higher is probability that the fractures intersect with each other and with the lateral sides of the domain of interest. Interestingly, curves of $\langle q \rangle / q_0$ exhibit two different behaviors. For $\langle R \rangle / R_0 < 1$, i.e. under-estimation of the mean radius of the fractures, there is very little variability between of flux from the lateral surface of the domain, however when $\langle R \rangle / R_0 > 1$ the variability between the fluxes is more pronounced. Indeed, when the mean radius of the fractures is over-estimated, i.e. larger than the "true" mean radius, the connected flow path between the injection segment and the lateral sides of the domain is more tortuous and continuous horizontally which leads to a more asymptotic behavior of $\langle q \rangle / q_0$ as function of $\langle R \rangle / R_0$. In fact, the water has 4 possibilities to escape the domain horizontally but only two possibilities (top, and bottom) in the vertical direction which explains the pronounced differences between the curves at larger $\langle R \rangle / R_0$ (Figure 8).

Moreover, it is worth noting that a 20% under-estimation of $\langle R \rangle$ can lead to 50% under-estimation in $\langle q \rangle$, on the other hand a 20% over-estimation of $\langle R \rangle$ can lead to 50% to 200% increase in the $\langle q \rangle$, in the horizontal and vertical direction, respectively. For $\langle R \rangle / R_0$ less than 50%, the probability that the fractures are connected between themselves and to the boundary domain is below the percolation threshold (Charlaix et al., 1984). Therefore, $\langle q \rangle / q_0$ vanishes. For completeness the 1st moments are

plotted on Figure 8 (Top) using both linear-linear and linear-log scale. A closer look at the normalized 2nd moment σ^2_q/σ^2_0 (bottom Figure 8) curves, one concludes that the variability between the curves is minimal. A 20% under-estimation of <R> leads to 20% under-estimation of the variance of the fluxes. However, a 20% over-estimation of <R> can triple the variance of the "ground-truth" flux variance.

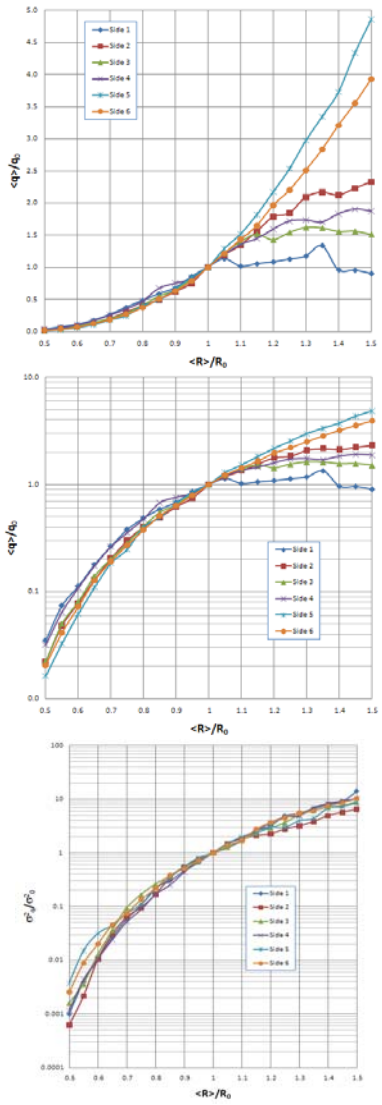

Figure 8: Statistical 1st (Top: lin-lin, Middle: lin-log scales) and 2nd moments (Bottom: lin-log scale) of the fluxes from the 6 different sides of the simulated domain, case I.

Case II: Mixed 1st & 2nd type boundary conditions

Similar analysis for Case II (Figure 6b) has been conducted and results of the 1st and 2nd moments are plotted as function of the scaling ratio $<R>/R_0$ on Figure 9.

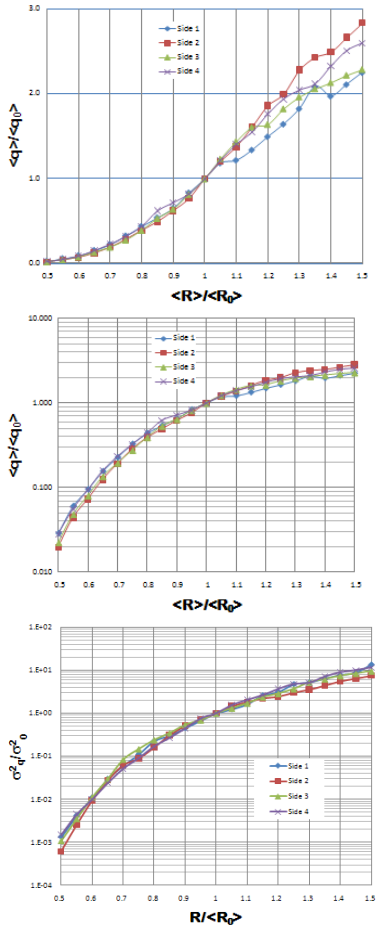

Figure 9: Statistical 1st (Top: lin-lin, Middle: lin-log scales) and 2nd moments (Bottom: lin-log scale) of the fluxes from the 4 different sides of the simulated domain, case II.

Similar conclusions to Case I can be drawn for case II. In line with the previous analysis, because the water is restricted by the top and bottom sides of the domain, injected water can only escape through side 1 to Side 4 which further limit the variability between the spatial variability of fluxes. Moreover, because the flow path restrictions, the magnitude of $<q>/q_0$ are larger than those obtained in Case I. Indeed, water that has escaped through top and bottom sides of the domain in Case I, now is forced to leave only through the later surfaces in Case II. On the contrary, the variance has not changed significantly, except that the variability between the curves has been reduced.

Correlations between $<q>/q_0$, σ^2_q/σ^2_0 & $<R>/R_0$

A preliminary analysis of the correlation between the 1st and 2nd moments as function of $<R>/R_0$ reveals two distinct cases. On one hand, for $<R>/R_0$ less than 1, $<q>/q_0$ is proportional to $(<R>/R_0)^2$, while σ^2_q/σ^2_0 is proportional to $(<R>/R_0)^3$. On the other hand, when $<R>/R_0$ greater than 1, $<q>/q_0$ is proportional to $(<R>/R_0)^1$, while σ^2_q/σ^2_0 is proportional to $(<R>/R_0)^2$. In both cases, the ratio $<q>/q_0$ exhibits a correlation

to $<R>/R_0$ one order less than the correlation between σ^2_q/σ^2_0 and $<R>/R_0$. More detailed theoretical analysis, using expansion techniques, and numerical simulations are in progress and they will be presented in a subsequent paper.

Effective property tensors

In order to assess the impact of $<R>/R_0$ on the overall anisotropy of the fracture network, a first order analysis of the effective hydraulic conductivity tensor is conducted. In fact, given a specified pressure (head) gradient between the injection segment and the 6 or 4 specified sides of the domain for Case I and II, respectively, and given the flux <q> for each side, the effective hydraulic conductivity tensor is given by: $K_{eff} = <q>/grad(H)$. The gradient, grad (H), can be estimated as the head drop over the average distance between the injection segment and the sides of the domain, <q> has already been calculated and presented in the previous subsection, and therefore the determination of K_{eff} is straightforward. Furthermore, we can calculate the effective K_0 of the "ground-truth" case, specifically when $<R>= R_0$, under the same boundary conditions for Case I and II, i.e. $K_0 = q_0/grad(H)$. Consequently, $K_{eff}/ K_0=<q>/q_0$, which has previously been discussed. To better represent the principal directions of the tensor of hydraulic conductivity, we adopted a spider-web chart representation. Each side of the domain is labeled 1 through 6 and it is represented as an axis. Values of $<q>/q_0$ are then plotted for various $<R>/R_0$. The resulting plots are displayed on Figure 10a and Figure 11a for case I and II, respectively. Similarly, if we decompose <q> into q_0+q' and <K> into K_0+K', where < > are averages, and q' and K' are deviations from the "ground-truth" mean of q_0 and K_0 of the flux and the tensor of permeability, respectively; one can show that the σ^2_q is proportional to σ^2_K, which is the variance of the hydraulic conductivity tensor. Therefore, σ^2_K/ σ^2_0 is proportional to σ^2_q/σ^2_0 since σ^2_0 is a constant. Then σ^2_q/σ^2_0 is itself a surrogate of the statistical 2nd moment tensor of the hydraulic conductivity tensor. Values of σ^2_q/σ^2_0 are then plotted for various $<R>/R_0$. The resulting plots are displayed on Figure 10b and Figure 11b for case I and II, respectively.

Figures 10 & 11 show that over estimating <R> lead to anisotropy not only in the effective tensor of the hydraulic conductivity but also in the variance of the tensor of the hydraulic conductivity. More interestingly, the tensor of the effective conductivity may exhibit different principal directions than that of the tensor of the variance of the effective conductivity. Furthermore, Figure 11a shows that regardless the value of $<R>/R_0$ the system exhibit a very small anisotropy of the tensor K and the system could be considered as isotropic, however the variance of the tensor K clearly display a strong anisotropic behavior with major principal direction oriented toward Side 1 and minor direction toward Side 2. Mechanical stimulation of fracture depends not only on the tensor of the hydraulic conductivity and it is main principal directions but also on the tensor of the variance of the hydraulic conductivity tensor and its principal directions. The latter is usually neglected in predicting fracture stimulation.

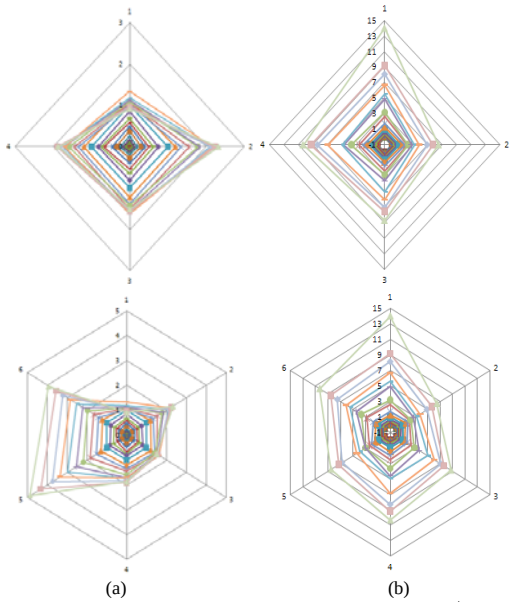

(a) (b)

Figure 10: Spider-web chart for the statistical 1st (Top a) and 2nd (Top b) moments for the 4 lateral sides of the domain (axises labeled 1 through 4). Each colored curve correspond to a specific $<R>/R_0$. Similar plots are given at the bottom (a & b) for all 6 sides of the domain including bottom side (labeled 5) and top side (labeled 6).

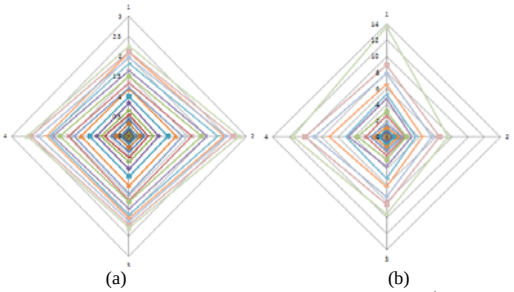

(a) (b)

Figure 11: Spider-web chart for the statistical 1st (a) and 2nd (b) moments for the 4 lateral sides of the domain (axises labeled 1 through 4). Each colored curve correspond to a specific $<R>/R_0$.

CONCLUSIONS

Throughout the present paper we have attempted to address the impact of geological characterization uncertainty on the flow field characteristics in stochastic discrete fracture network approach. Because the size of the fractures is by far the most

difficult parameter to infer from borehole data, we have investigated its uncertainty on the 1st and 2nd moment of the flow field (fluxes). It has been found that under-estimating the mean radius (size) of fractures may have negative consequences on the variability of the flow field. Furthermore, the effective conductivity tensor may exhibit anisotropy or isotropy which depends not only on the size of the fractures but also on the boundary conditions of the conceptual model. More interestingly, the major and minor principal directions of the tensor of the conductivity do not necessarily coincide with the principal directions of the tensor of the variance of the conductivity tensor; both are necessary quantities for the risk analysis and the reliability of an EGS design, especially when predicting induced microseismicity.

Despite that geothermal energy is a mature geosciences energy technology and more emerging novel approaches have been proposed, and some have been conceptually analyzed (e.g. alternative heat-transfer fluids) the main problems in EGS remain still the same. More considerable attention need to be focused on the fracture characterization originated by natural causes or anthropogenically induced.

REFERENCES

Barker J.A., The reciprocity principle and an analytical solution for Darcian flow in a network. *Water Resour. Res.*, 27(5), pp. 743-746, 1991.

Brown, D., 2000. A Hot Dry Rock geothermal energy concept utilizing supercritical CO2 instead of water. In: Proceedings of the Twenty-Fifth Workshop on Geothermal Reservoir Engineering, Stanford University, pp. 233–238, 2000.

Charlaix E., E. Guyon, N. Rivier, A criterion for percolation threshold in a random array of plates. *Solid State Communications*, 50(11), 999-1002, 1984.

Dershowitz W.S. and H.H. Einstein, Characterizing Rock Joint Geometry with joint system models. *Rock Mechanics and Rock Engineering* 21, 21-51, 1988.

Ezzedine S., G. de Marsily, Study of transient flow in hard fractured rocks with a discrete fracture network model. *Int. J. Rock Mech. Min. Sci. & Geomech. Abstr.*, 30(7), pp. 1605-1609, 1993.

Ezzedine, S., 1994, Modeling flow and transport in fractured media using continuum and SDFN approaches. Application to HDR geothermal reservoirs (in French). Ph.D. Thesis, Ecole des Mines de Paris, France, 208p. 1994

Ezzedine S., Stochastic Modeling of Flow and Transport in Porous and Fractured Media. *Chapter 154 in Encyclopedia of Hydrological Sciences*, 34pages, Willey 2005

Ezzedine, S., 2008, Coupled THMC processes in Geological Media using Stochastic Discrete Fractured Network. Application to HDR Geothermal Reservoirs. Eos Transactions AGU, 89(53), Fall Meeting Supplement, Abstract H41A-084, 2008

Fujii, H., R. Itoi, J. Fujii and Y. Uchida, 2005, Optimizing the design of large-scale ground-coupled heat pump systems using groundwater and heat transport modeling, *Geothermics* **34** (2005), pp. 347364.

Gherardi, F., G. Gianelli, T. Xu, K. Pruess, 2008, Gas-water-rock interactions at Mt. Amiata geothermal field as natural analogues for enhanced geothermal systems (EGS) operated with CO2. In 17th International conference on Computational Methods in Water Resources, San Francisco, July 6-10, 2008.

Kaieda, A. Ueda, H. Wakahama, S. Mito, K. Sugiyama, A. Ozawa, Y. Kuroda, H. Sato, T. Yajima, K. Kato, K. Kubota and Y. Kaji, 2009; Field Experiments for Studying on CO2 Sequestration in Solid Minerals at the Ogachi HDR Geothermal Site, Japan. 34rd Stanford Workshop on Geothermal Reservoir Eng. 2009

Nalla, Gopi, G. Michael Shook, Gregory L. Mines, and K. Kit Bloomfield. 2004, Parametric Sensitivity Study of Operating and Design Variables in Wellbore Heat Exchangers. May 2004. Idaho National Engineering and Environmental Laboratory. Idaho Falls, Idaho.

Porras, E. A., T. Tanaka, H. Fujii, R. Itoi 2007, **Error! Hyperlink reference not valid.**. Geothermics, Volume 36, Issue 4, August 2007, Pages 304-329

Pruess K, 2006, Enhanced geothermal systems (EGS) using CO2 as working fluid—A novel approach for generating renewable energy with simultaneous sequestration of carbon, Geothermic 35(4), 351-367, 2006.

Pruess K; Spycher, N; 2008; On the development of EGS with CO2 as heat transmission fluid. Computational Methods in Water Resources, San Francisco, 2008

Talbot A., The accurate numerical inversion of Laplace transforms. *Int. J. Int. Math. Appl.*, 23, 97-120, 1979.

Tenma, N., K. Yasukawa and G. Zyvoloski, 2003, Model study of the thermal storage system by FEHM code, Geothermics 32 (2003), pp. 603607.

Acknowledgments:

This work performed under the auspices of the U.S. Department of Energy by Lawrence Livermore National Laboratory under Contract DE-AC52-07NA27344. LLNL-PROC-422871-DRAFT